

# Cold collisions involving rotationally hot oxygen molecules

K. Tilford, M. Hoster, P. M. Florian, and R. C. Forrey

*Pennsylvania State University, Berks-Lehigh Valley College, Reading, Pennsylvania 19610-6009, USA*

(Received 29 August 2003; published 12 May 2004)

Cold and ultracold collisions involving rotationally hot oxygen molecules are investigated using quantum-mechanical, coupled-channel, coupled-states, and effective-potential scattering formulations. Quenching rate coefficients are given for initial rotational levels near the dissociation threshold. The stability of the oxygen “super rotors” against collisional decay is compared to previous investigations involving hydrogen molecules where the rotational inertia was significantly smaller. In contrast to hydrogen, all possible states of rotationally hot oxygen are quenched very rapidly during a collision with a buffer gas helium atom, and the quenching efficiency is always dominated by pure rotational transitions.

DOI: 10.1103/PhysRevA.69.052705

PACS number(s): 34.50.Ez

## I. INTRODUCTION

Experimental schemes to produce diatomic molecules in highly excited rotational states have been proposed [1,2] and recently realized [3]. Theoretical studies have suggested that the collisional dynamics of such rotationally hot molecules would be particularly interesting at low temperatures [4–8]. For example, it has been demonstrated that rotationally excited hydrogen molecules may undergo rapid quenching during cold collisions with a helium atom due to quasiresonant vibration-rotation (QRVR) transitions [4,5]. Alternatively, hydrogen “super rotors” in certain states may experience virtually no collisional quenching at all [6,8]. The fate of the molecule depends only on its initial rovibrational state and whether a nearby QRVR transition is energetically allowed. This all-or-nothing behavior produces sharp structures in the rotational distribution of total quenching rate coefficients [4,5]. It is natural to consider whether other diatomic systems would exhibit a similar kind of quenching behavior during a cold or ultracold collision. Some preliminary studies were performed for rotationally excited oxygen molecules [8]. It was found that all states with rotational level  $j$  less than 40 would be rapidly quenched in collision with a buffer gas helium atom due to pure rotational deexcitation. However, this is not a fair comparison of the near-dissociation collisional dynamics, which is where one might expect similar interesting behavior to occur. While the hydrogen molecule is fully dissociated by  $j=40$ , the oxygen molecule must be excited to  $j=120$  or so before comparable QRVR transitions are accessible and to  $j \approx 160$  before any interesting near-dissociation behavior might occur [8]. Unfortunately, the numerically exact coupled-channel (CC) scattering formulation becomes intractable as the rotational levels are increased to such large values. Alternative formulations such as the coupled states (CS) and effective-potential (EP) approximations offer a possible means to compute the desired large- $j$  scattering data. However, it is necessary to establish the applicability of CS and EP approximations in the cold and ultracold temperature regime. In this work, we calculate CC, CS, and EP cross sections for rotational levels where each formulation is able to produce results. After determining the accuracy of the approximate methods, we extend the calculations all the way to dissociation.

We also investigate the translational energy dependence of the cross sections and rate coefficients, extending previously published results [9] to include highly rotationally excited initial states. Oxygen molecules are open shell with electron spin equal to one (this is responsible for its paramagnetism). Therefore, there exists a nonzero coupling between the electron spin and the nuclear rotational angular momentum. As in previous studies [9,10,11] we assume that this coupling is small compared to the potential energy and its anisotropy. Paramagnetic molecules such as oxygen offer possibilities for buffer gas cooling and trapping [12]. Consequently, ultracold collisions of oxygen molecules with helium atoms [9,13] and with other oxygen molecules [14] have been reported recently. The present results add to this body of work. It also provides a point of comparison to the rotational quenching studies of hydrogen molecules [6,8] and molecular ions [15], and with rotational resonance studies [16,17] at ultracold temperatures. For hydrogen molecules, the rotational distribution of zero-temperature quenching rate coefficients revealed a qualitative structure that was independent of the colliding partner [18]. Therefore, we expect that the qualitative features obtained here for a helium collision partner would likely extend to other buffer gas atoms or molecules. In the following section, we review the CC formulation that will allow us to determine the accuracy of the CS and EP approximations in the ultracold temperature limit.

## II. COUPLED-CHANNEL FORMULATION

The atom-diatom Hamiltonian in the center-of-mass frame is given by

$$H = -\frac{1}{2m}\nabla_r^2 - \frac{1}{2\mu}\nabla_R^2 + v(r) + V_I(r, R, \theta), \quad (1)$$

where  $r$  is the distance between the oxygen atoms,  $R$  is the distance between the helium atom and the center of mass of the diatom,  $\theta$  is the angle between  $r$  and  $R$ ,  $m$  is the reduced mass of the diatom, and  $\mu$  is the reduced mass of the helium atom with respect to the diatom. The three-dimensional potential energy surface is separated into a diatomic potential  $v(r)$  and an interaction potential  $V_I(r, R, \theta)$ . The diatomic Schrödinger equation

$$\left[ \frac{1}{2m} \frac{d^2}{dr^2} - \frac{j(j+1)}{2m r^2} - v(r) + \epsilon_{vj} \right] \chi_{vj}(r) = 0 \quad (2)$$

is solved by expanding the rovibrational wave function  $\chi_{vj}(r)$  in a Sturmian basis set. The full wave function is expanded in a set of channel functions [ $n \equiv (vjl)$ ]:

$$\Psi^{JM}(\vec{R}, \vec{r}) = \frac{1}{R} \sum_n C_n(R) \phi_n(\hat{R}, \vec{r}), \quad (3)$$

$$\phi_n(\hat{R}, \vec{r}) = \frac{1}{r} \chi_{vj}(r) \sum_{m_j} \sum_{m_l} (j|J|m_j, M - m_l) Y_{m_j}^j(\hat{r}) Y_{m_l}^l(\hat{R}), \quad (4)$$

where  $l$  is the orbital angular momentum of the atom with respect to the diatom,  $J$  is the total angular momentum,  $M$  is the projection of  $J$  onto the space-fixed  $z$  axis, and  $(j|J|m_j, M - m_l)$  denotes a Clebsch-Gordon coefficient. Operating the Hamiltonian (1) on the channel functions (3) leads to a set of coupled equations,

$$\left[ \frac{d^2}{dR^2} - \frac{l_m(l_m+1)}{R^2} + 2\mu E_m \right] C_m(R) = \sum_n C_n(R) \langle \phi_m | U_I | \phi_n \rangle, \quad (5)$$

where  $E_m$  is the translational energy and  $l_m$  is the orbital angular momentum in the  $m$ th channel. The reduced interaction potential  $U_I$  is expanded in Legendre polynomials,

$$U_I(R, r, \theta) = 2\mu V_I(R, r, \theta) = \sum_{\lambda=0}^{\infty} U_{\lambda}(R, r) P_{\lambda}(\cos \theta) \quad (6)$$

and the solution to Eq. (5) is matched asymptotically to free waves to obtain the scattering matrix  $S_{vj;v'j'l'}^J$ . The cross sections are given by [19]

$$\sigma_{vj \rightarrow v'j'} = \frac{\pi}{2\mu E_{vj}} (2j+1) \sum_{J=0}^{\infty} \sum_{l=|J-j|}^{|J+j|} \sum_{l'=|J-j'|}^{|J+j'|} |\delta_{jj'} \delta_{ll'} \delta_{vv'} - S_{vj;v'j'l'}^J|^2. \quad (7)$$

Inspection of Eq. (7) reveals the difficulty of using the CC approach for rotationally hot molecules. The dimensionality of the scattering matrix grows rapidly with increasing  $j$  due to the exact treatment of the angular-momentum coupling. For typical molecules (i.e., any molecule other than hydrogen) the highly rotationally excited near-dissociation dynamics will require a decoupling approximation in order to obtain a numerical result.

### III. DECOUPLING APPROXIMATIONS

The coupled states (CS) approximation [20,21] begins with

$$\Psi^{J\Omega}(\vec{R}, \vec{r}) = \frac{1}{R} \sum_{v,j} C_{vj}(R) \chi_{vj}(r) Y_{j\Omega}(\theta, 0), \quad (8)$$

where  $\Omega$  is the body-fixed projection of both  $J$  and  $j$ . The centrifugal term in the total Hamiltonian will give diagonal matrix elements proportional to  $J(J+1) + j(j+1) - 2\Omega^2$ . The CS approximation is made by neglecting the off-diagonal Coriolous couplings that arise in the body-fixed frame. Different variations of the CS approximation have recently been studied by Krems [22]. It was found that the  $J$  labeled variant introduced by Pack [20] performed best for He+CO collisions at ordinary temperatures [22]. This version does not generally allow  $s$ -wave scattering for rotationally excited states of the diatom. Therefore, we use the  $l$ -labeled variant originally proposed by McGuire and Khouri [21] which assumes that the diagonal eigenvalue of the orbital angular-momentum operator  $\hat{l}^2$  is approximated by  $l(l+1)$  where  $l$  is a conserved quantum number. This procedure allows  $s$ -wave scattering and yields the set of coupled equations

$$\left[ \frac{d^2}{dR^2} - \frac{l(l+1)}{R^2} + 2\mu E_{vj} \right] C_{vj}(R) = \sum_{v'j'} C_{v'j'}(R) \times \langle vj\Omega | U_I | v'j'\Omega \rangle, \quad (9)$$

where

$$\langle vj\Omega | U_I | v'j'\Omega \rangle = \sum_{\lambda=0}^{\lambda_{max}} (-1)^{\Omega} [(2j+1)(2j'+1)]^{1/2} \times \begin{pmatrix} j' & \lambda & j \\ 0 & 0 & 0 \end{pmatrix} \begin{pmatrix} j' & \lambda & j \\ \Omega & 0 & -\Omega \end{pmatrix} \langle \chi_{vj} | U_I | \chi_{v'j'} \rangle. \quad (10)$$

The  $(\cdots)$  denotes a  $3j$  symbol and the  $\{\cdots\}$  below denotes a  $6j$  symbol. Equation (9) shows that the CS formulation requires a set of calculations for each value of  $\Omega$ . The EP formulation is independent of  $\Omega$  with potential matrix elements given by [23]

$$\langle vj | U_I | v'j' \rangle = \sum_{\lambda=0}^{\lambda_{max}} \left[ \frac{(-1)^{j+j'+|j-j'|}}{(2\lambda+1)} \sqrt{(2j+1)(2j'+1)} \right]^{1/2} \times \begin{pmatrix} j' & \lambda & j \\ 0 & 0 & 0 \end{pmatrix} \langle \chi_{vj} | U_I | \chi_{v'j'} \rangle. \quad (11)$$

In the CS and EP formulations, the orbital angular momentum of the atom is decoupled from the orbital angular momentum of the diatom and is assumed to be a conserved quantity. Therefore, the number of channels is the same as the number of states ( $v, j$ ). The CS potential matrix element (10) and the EP matrix element (11) are considerably simpler than the CC potential matrix element

$$\langle vjl|U_I|v'j'l'\rangle = \sum_{\lambda=0}^{\lambda_{max}} (-1)^{j+j'-J} [(2j+1)(2j'+1)(2l+1) \\ \times (2l'+1)]^{1/2} \begin{Bmatrix} J & l & j \\ \lambda & j' & l' \end{Bmatrix} \begin{pmatrix} j' & \lambda & j \\ 0 & 0 & 0 \end{pmatrix} \\ \times \begin{pmatrix} l' & \lambda & l \\ 0 & 0 & 0 \end{pmatrix} \langle \chi_{vj}|U_\lambda|\chi_{v'j'} \rangle \quad (12)$$

whose dimension increases rapidly with  $j$ . The CS and EP approximations require matching the solution of Eq. (9) to asymptotic free waves to obtain the respective scattering matrices  $S_{vj;v'j'}^{\Omega}$  and  $S_{vj;v'j'}^l$ . The collision cross section (7) may then be replaced by the respective CS or EP cross section:

$$\sigma_{vj \rightarrow v'j'} = \frac{\pi}{2\mu E_{vj}} \sum_{J=0}^{\infty} (2J+1) \sum_{\Omega=0}^{\Omega_{max}} (2 - \delta_{\Omega 0}) |\delta_{jj'} \delta_{vv'} - S_{vj;v'j'}^{\Omega}|^2, \quad (13)$$

$$\sigma_{vj \rightarrow v'j'} = \frac{\pi}{2\mu E_{vj}} \sum_{l=0}^{\infty} (2l+1) |\delta_{jj'} \delta_{vv'} - S_{vj;v'j'}^l|^2. \quad (14)$$

The set of coupled equations (5) and (9) may be conveniently solved using the general inelastic scattering program MOLSCAT [24]. The rate coefficients may be obtained from the usual thermal averaging procedure

$$R_{vj \rightarrow v'j'}(T) = (8k_B T / \pi \mu)^{1/2} \frac{1}{(k_B T)^2} \int_0^\infty \sigma_{vj \rightarrow v'j'}(E_k) \\ \times \exp(-E_k/k_B T) E_k dE_k, \quad (15)$$

where  $T$  is the temperature and  $k_B$  is the Boltzmann constant. The total quenching rate coefficients  $R_{vj}(T)$  are given by

$$R_{vj}(T) = \sum_{v'j'} R_{vj \rightarrow v'j'}(T). \quad (16)$$

The sum in Eq. (16) includes contributions from all possible exit channels. The total quenching rate coefficient is an important quantity in cooling and trapping experiments. Typically, the ratio of the elastic rate coefficient to the total quenching rate coefficient must be very large in order for a collisional cooling scheme (e.g., buffer gas cooling, evaporative cooling) to be effective. Otherwise, the energy released in the deexcitation process will lead to unwanted heating of the gas and limit further cooling efforts.

#### IV. RESULTS

Figures 1 and 2 show zero-temperature cross sections and rate coefficients for  ${}^3\text{He} + \text{H}_2$ . The details of the CC calculations are the same as those reported previously [8] so will not be repeated here. The CS results were computed by restricting  $\Omega=0$  in Eq. (10) as suggested by Krems [25]. This procedure yields cross sections that are qualitatively similar to the more accurate CC results for both elastic and inelastic scattering. The EP results are less accurate than CS for this system, however, the qualitative behavior is still quite similar

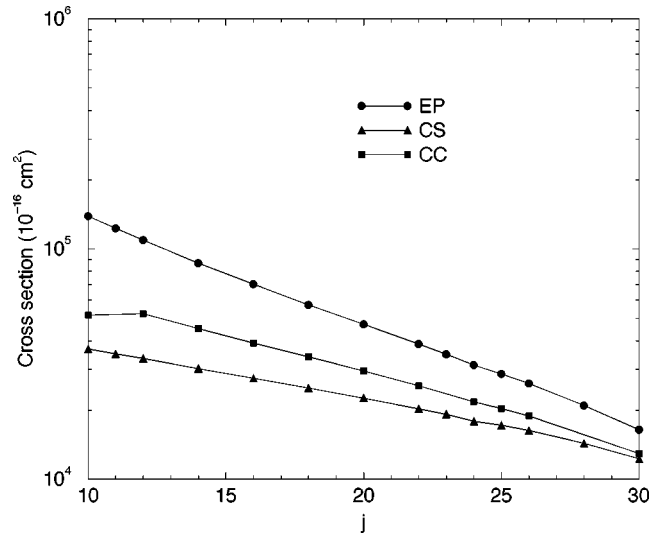


FIG. 1. Elastic scattering cross sections for  ${}^3\text{He} + \text{H}_2$  in the limit of zero temperature. In each calculation the molecule is initially in the  $v=0$  vibrational level with initial rotational quantum number  $j$ .

to the CC results, particularly for the inelastic cross sections. The elastic cross sections generally appear to be more sensitive to the decoupling approximations than the corresponding inelastic cross sections. The accuracy of the CS inelastic cross sections is about the same when  $\Omega$  is summed over as it is when  $\Omega$  is restricted to zero. In the results that follow, a sum over all possible  $\Omega$  was used for the cross sections obtained by the CS approximation, unless stated otherwise.

For  ${}^3\text{He} + \text{O}_2$ , we have performed our scattering calculations using the potential energy surface of Groenenboom and Struniewicz [26]. For the oxygen diatom, we used the potential of Friedman [27] as modified by Babb and Dalgarno

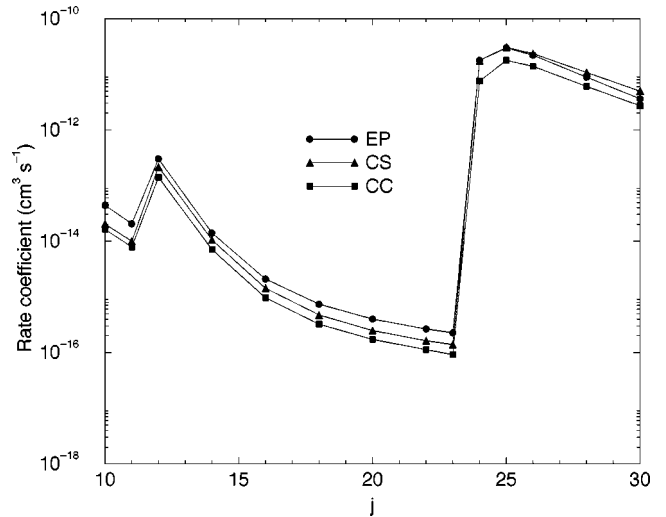


FIG. 2. Rate coefficients for total inelastic quenching for  ${}^3\text{He} + \text{H}_2$  in the limit of zero temperature. In each calculation the molecule is initially in the  $v=0$  vibrational level with initial rotational quantum number  $j$ . The peaks at  $j=12$  and  $j=24$  are due to the opening of the  $\Delta j=-4\Delta v$  and  $\Delta j=-2\Delta v$  transitions. The EP and CS approximations are able to reproduce the shape of the more accurate CC calculations.

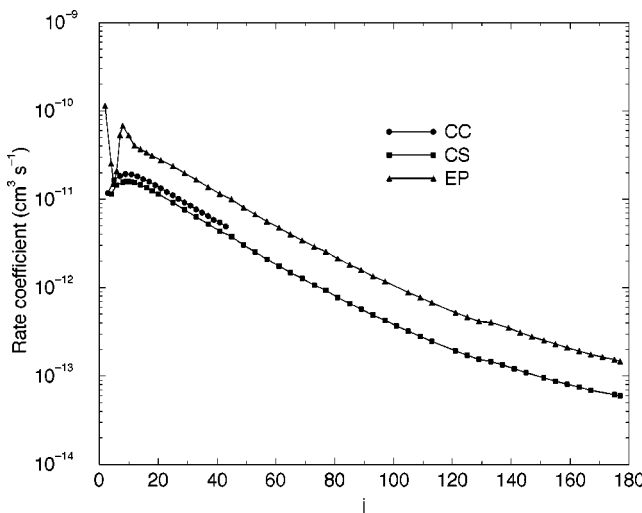


FIG. 3. Rate coefficients for total inelastic quenching for  ${}^3\text{He} + \text{O}_2$  in the limit of zero temperature. The CC and CS results are smoothly varying with a maximum value at  $j=10$ . The EP results show a strong nonphysical oscillation for low values of  $j$ . The CS data slightly underestimates the rate coefficients while the EP data are nearly a factor of 2 greater than the CC results for large  $j$ .

[28]. In all of our calculations, the anisotropy of the potential energy surface was well described using  $\lambda_{max}=10$ , and 20 integration nodes for  $0 < \theta < 90^\circ$ . Pure rotational transitions were converged to within a few percent for basis sets restricted to  $j-10 \leq j \leq j+2$  with  $v_{max}=1$ . Rovibrational transitions required additional rotational channels to be included, so we have conservatively restricted the basis set to  $j-20 \leq j \leq j+2$  where  $j$  is the initial level of interest. Figure 3 shows the total quenching rate coefficient  $R_{0j}(T \rightarrow 0)$  as a function of  $j$ . The numerically exact CC results are given along with approximate CS and EP results. The CC and CS results are smoothly varying with a maximum value at  $j=10$ . The EP results show a strong nonphysical oscillation for  $j < 15$ . For  $j > 15$ , the EP results settle down and become smoothly varying with  $j$ . The CS data slightly underestimates the rate coefficients while the EP data are nearly a factor of 2 greater than the CC results for large  $j$ . Although it was not possible to perform CC calculations for  $j > 40$ , the CS and EP formulations allowed us to obtain converged results for all possible values of  $j$ . Because the total quenching rate coefficients are dominated by pure rotational  $\Delta j=-2$  transitions, it is possible to extrapolate the CC results and fit the  $j > 20$  data for each scattering formulation using

$$\lim_{T \rightarrow 0} R_{vj}(T) = A \exp(\Delta E/B), \quad (17)$$

where  $\Delta E$  is the energy gap between the initial and final rotational levels. The exponential scale parameter  $B$  is  $140.845 \text{ cm}^{-1}$  and the coefficient  $A$  is 1.5, 3.5, and  $2.0 \times 10^{-11} \text{ cm}^3 \text{s}^{-1}$  for CS, EP, and CC respectively.

Figure 4 shows the rate coefficients for rovibrational transitions in which the vibrational level is increased by one unit. Both CS results ( $\Omega_{max}=0$  and  $\Omega_{max}=j+2$ ) show a similar structure with sharp increases occurring at the opening of a

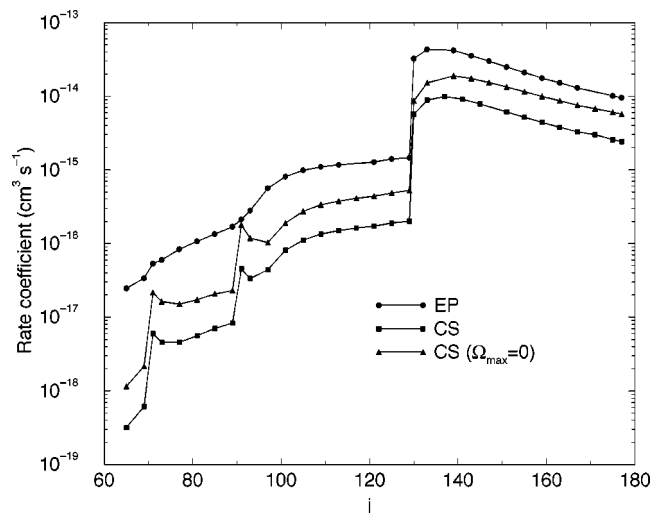


FIG. 4. Rate coefficients for  $\Delta v=1$  transitions in the limit of zero temperature. CS calculations were performed using  $\Omega_{max}=0$  and  $\Omega_{max}=j+2$ . Both CS calculations show similar structure with sharp increases occurring at the opening of a new channel. The  $\Delta j=-8$  transition becomes energetically allowed at  $j \geq 71$ , the  $\Delta j=-6$  transition at  $j \geq 91$ , and the  $\Delta j=-4$  transition at  $j \geq 130$ . The molecule dissociates before the  $\Delta j=-2$  transition becomes energetically allowed. The EP results show less structure at the low  $j$  thresholds but qualitatively similar behavior to CS as  $j$  is increased.

new channel. The  $\Omega_{max}=0$  calculations provide a factor of  $j$  speedup over the full CS calculations and are comparable in speed to the EP calculations. The EP results show less structure at the low  $j$  thresholds but qualitatively similar behavior to CS as  $j$  is increased. The  $\Delta j=-8$  transition becomes energetically allowed at  $j \geq 71$ , the  $\Delta j=-6$  transition at  $j \geq 91$ , and the  $\Delta j=-4$  transition at  $j \geq 130$ . A very small discontinuity may be seen in Fig. 3 at  $j=130$  due to the  $\Delta j=-4$  transition which provides a small contribution to the total quenching rate coefficient. The molecule dissociates before the  $\Delta j=-2$  transition becomes energetically allowed. The rotational distribution of zero-temperature rate coefficients given in Fig. 4 is reminiscent of the staircase plot for the fixed  $\Delta j/\Delta v$  ratios that was found in classical trajectory studies of QRVR transfer [29]. The structure is a consequence of the balance between energy and angular-momentum constraints [30] and appears to be a universal feature of atom-diatom collisions independent of the specific system. However, the distribution may appear differently for each system. For example, in Fig. 2 the rate coefficients for  $\text{He} + \text{H}_2$  show a sharp increase at the opening of a QRVR transition followed by a smooth decrease with  $j$  until the next QRVR transition is energetically accessible. Figure 4 shows that the rate coefficients for  $\text{He} + \text{O}_2$  are much flatter in between the different thresholds but become more like the  $\text{H}_2$  results as  $j$  increases. This is because the transitions become more specific and efficient as the angular-momentum gap is reduced. The smooth decrease with  $j$  following a QRVR threshold is a consequence of the increasing energy gap between the initial and final rovibrational levels. The issue of whether the sharp increase plays an important role in the rotational relaxation depends on the magnitude of the rovibrational rate coeffi-

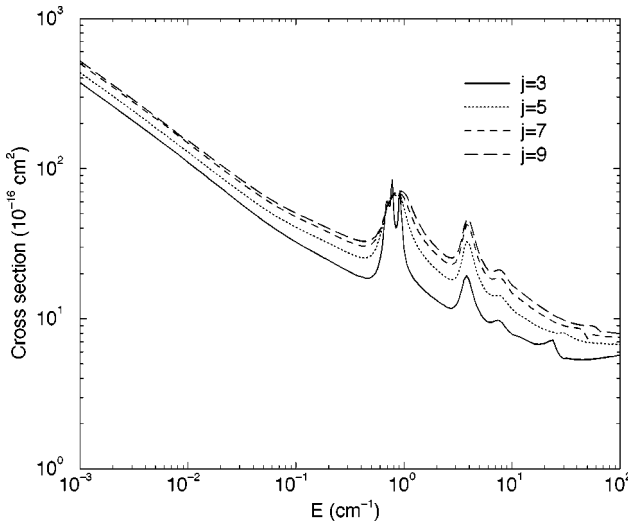


FIG. 5. Cross sections for the  $\Delta v=0, \Delta j=-2$  transition as a function of translational energy. The molecule is in the  $v=0$  level for all data shown and the calculations were performed using the CC formulation. Shape resonances occur at about the same translational energy for each initial  $j$  level. The Wigner threshold limiting  $E^{-1/2}$  behavior occurs for  $E < 10^{-2} \text{ cm}^{-1}$ .

cents relative to the pure rotational rate coefficients. For hydrogen molecules, the pure rotational quenching rate coefficients were dominated by the rovibrational rate coefficients whenever QRVR transitions were energetically open. Figures 3 and 4 show that this is not the case for oxygen. The pure rotational quenching rate coefficients are always dominant for all  $j$  and the rovibrational transitions play a negligible role in the relaxation. In addition, the rotational quenching is quite large so it is clear that a super rotor made of oxygen would be much more fragile than one made of hydrogen.

Figure 5 shows cross sections for the  $\Delta v=0, \Delta j=-2$  transition as a function of the incident kinetic energy. The molecule is in the  $v=0$  level for all data shown. Shape resonances occur at about the same translational energy for each initial  $j$  level. The locations of the shape resonances are also the same as those reported previously [9] for the  $v=1, j=1$  level. The magnitudes of the cross sections shown in Fig. 5 are much greater than those given in Ref. [9] because of the availability of pure rotational quenching, which dominates over the less efficient rovibrational quenching. Wigner threshold  $E^{-1/2}$  behavior occurs for energies less than  $10^{-2} \text{ cm}^{-1}$ , in agreement with the cross sections given in Ref. [9].

Figure 6 shows the rate coefficients for the  $\Delta v=0, \Delta j=-2$  transition as a function of temperature. The molecule is in the  $v=0$  level for all data shown. The shape resonances in the cross sections (see Fig. 5) give rise to steps in the rate coefficients for temperatures around 1–10 K. The Wigner threshold limiting behavior occurs for  $T < 10^{-2} \text{ K}$  yielding very efficient ultracold quenching rate coefficients of about  $10^{-11} \text{ cm}^3 \text{ s}^{-1}$ , in agreement with the results shown in Fig. 3. All data shown in Fig. 5–7 were computed using the CC scattering formulation. Figure 7 shows cross sections for elastic scattering as a function of translational energy. The molecule is in the  $v=0$  level with  $j=3, 5, 7$ , and 9. The

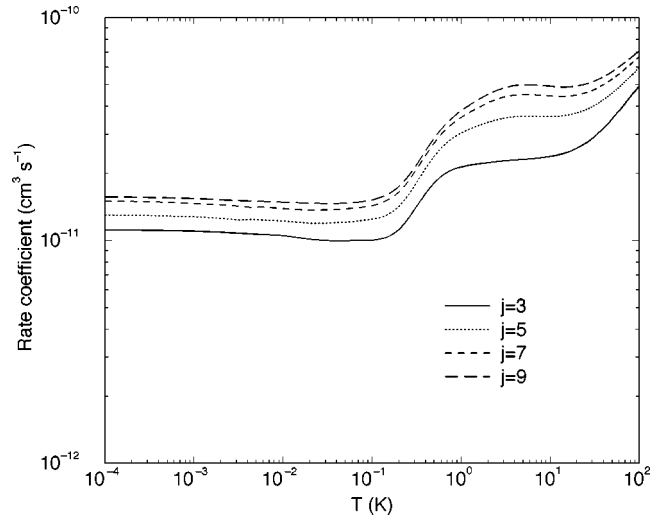


FIG. 6. Rate coefficients for the  $\Delta v=0, \Delta j=-2$  transition as a function of temperature. The molecule is in the  $v=0$  level for all data shown. The shape resonances in the cross sections give rise to steps in the rate coefficients for temperatures around 1–10 K. The Wigner threshold limiting behavior occurs for  $T < 10^{-2} \text{ K}$ .

Wigner threshold law for elastic scattering requires the cross section to approach a constant value as the collision energy tends to zero. This occurs for energies below  $10^{-3} \text{ cm}^{-1}$  which is a factor of 10 lower than the onset of inelastic threshold behavior. Structure in the elastic cross section due to shape resonances occurs just below  $1 \text{ cm}^{-1}$  as in the case of inelastic scattering (see Fig. 5). A similar structure was found [9] at this energy for  $j=0$  as were the oscillations in the cross section for energies between 1 and  $10 \text{ cm}^{-1}$ . The zero-energy cross section for elastic scattering is extremely small, typically around  $10 \text{ Å}^2$  for the rotational levels shown in Fig. 7. This is more than 500 times smaller than the zero-energy elastic cross section for hydrogen molecules [5] and

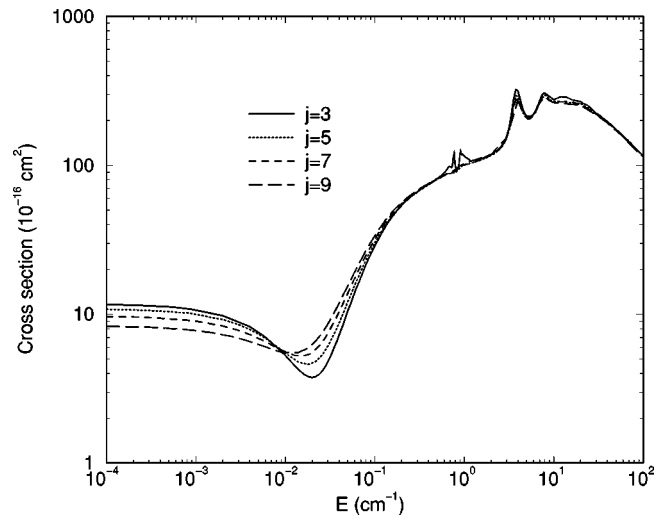


FIG. 7. Cross sections for elastic scattering as a function of translational energy. The molecule is in the  $v=0$  level for all data shown and the calculations were performed using the CC formulation.

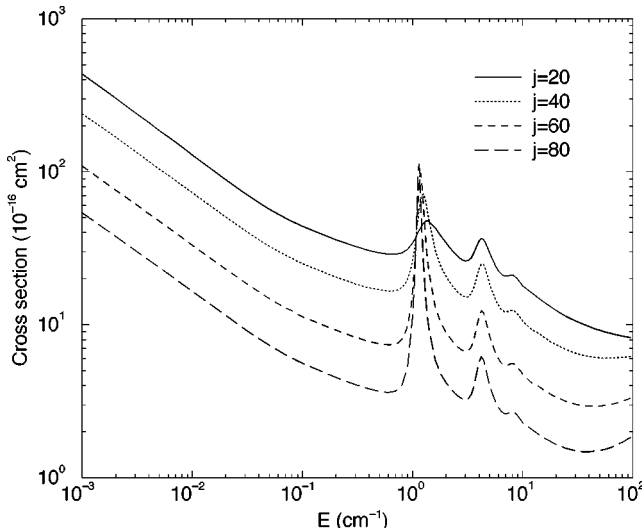


FIG. 8. Cross sections for the  $\Delta v=0, \Delta j=-2$  transition as a function of translational energy. The molecule is in the  $v=0$  level and the calculations were performed using the EP approximation. The shape resonances near  $1$  and  $4\text{ cm}^{-1}$  are due to  $l=4$  and  $l=5$  centrifugal barriers, respectively.

suggests that collisional cooling would be very difficult for oxygen molecules even in the absence of inelastic quenching collisions.

Figure 8 shows cross sections for the  $\Delta v=0, \Delta j=-2$  transition as a function of energy. These cross sections were calculated using the EP approximation which allowed higher values of  $j$  to be considered. The curves appear to be very similar to those in Fig. 5 which were computed using the CC formulation. The shape resonances in the cross sections occur at the same energies as before. Because of the decoupling of angular momenta, the EP approximation allows for the resonant partial waves to be more easily identified. The strong resonances around  $1\text{ cm}^{-1}$  are due to the  $l=4$  centrifugal barrier, and the weaker resonances around  $4\text{ cm}^{-1}$  are a result of the  $l=5$  centrifugal barrier. Similar behavior was found using the CS approximation. Figure 9 shows the corresponding elastic cross sections for the EP calculations. Again, the curves appear to be very similar to those computed for smaller  $j$  using the CC formulation (see Fig. 7). The minima near  $0.02\text{ cm}^{-1}$  found in the CC elastic cross sections for low rotational levels are absent in the EP results for highly excited states. Although the decoupling approximations tend to be less reliable for elastic scattering, the EP and CS results suggest that the zero-energy elastic cross sections are even smaller for highly rotationally excited states than for the low-lying rotational states.

## V. CONCLUSIONS

We have investigated cold and ultracold collisions involving rotationally excited oxygen molecules using quantum-mechanical CC, CS, and EP scattering formulations. For large rotational levels, the CS and EP approximations give results that are within a factor of two of numerically exact CC results. This amount of error is acceptable considering

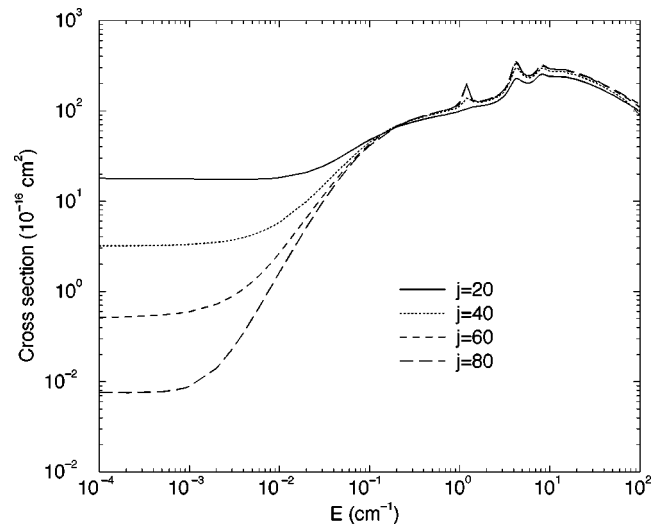


FIG. 9. Cross sections for elastic scattering as a function of translational energy. The molecule is in the  $v=0$  level and the calculations were performed using the EP approximation. The zero-energy elastic cross sections are extremely small for highly rotationally excited states.

the potential-energy surface is not designed for ultracold temperatures and the spin-rotation coupling has been neglected. The qualitative agreement between the three scattering formulations is encouraging, and we conclude that the decoupling approximations provide a means to obtain reliable estimates for states with large internal angular momentum. It is found that all possible states of rotationally hot oxygen are quenched very rapidly during a collision with a buffer gas helium atom, and the quenching efficiency is always dominated by pure rotational transitions. This finding is in contrast to rotationally hot hydrogen molecules, which has very low quenching efficiency when QRVR transitions are closed and very high quenching efficiency when QRVR transitions are open.

Although the quenching efficiency for QRVR transitions was found to be small for oxygen, a staircase plot was found for the rate coefficients as a function of rotational level. This feature of rovibrational transitions occurs as a result of the opening of new channels as the rotational level is increased. Resonances in the scattering cross sections were seen as a function of translational energy. The elastic cross section at low energy was very small for all rotational levels. The small elastic cross sections and the efficient pure rotational quenching behavior indicate that the near-dissociation dynamics of molecular oxygen would be less interesting and probably more difficult to study experimentally than the corresponding case of molecular hydrogen.

## ACKNOWLEDGMENTS

This work was funded by the National Science Foundation Grant Nos. PHY-0070920 and PHY-0244066. We thank Roman Krems for helpful communications.

- [1] J. Karczmarek, J. Wright, P. Corkum, and M. Ivanov, Phys. Rev. Lett. **82**, 3420 (1999).
- [2] J. Li, J. T. Bahns, and W. C. Stwalley, J. Chem. Phys. **112**, 6255 (2000).
- [3] D. M. Villeneuve, S. A. Aseyev, P. Dietrich, M. Spanner, M. Y. Ivanov, and P. B. Corkum, Phys. Rev. Lett. **85**, 542 (2000).
- [4] R. C. Forrey, N. Balakrishnan, A. Dalgarno, M. Haggerty, and E. J. Heller, Phys. Rev. Lett. **82**, 2657 (1999).
- [5] R. C. Forrey, N. Balakrishnan, A. Dalgarno, M. Haggerty, and E. J. Heller, Phys. Rev. A **64**, 022706 (2001).
- [6] R. C. Forrey, Phys. Rev. A **63**, 051403 (2001).
- [7] A. J. McCaffery, J. Chem. Phys. **113**, 10947 (2000).
- [8] R. C. Forrey, Phys. Rev. A **66**, 023411 (2002).
- [9] N. Balakrishnan and A. Dalgarno, J. Phys. Chem. **105**, 2348 (2001).
- [10] V. Aquilanti, D. Ascenzim, M. de Castro Vitores, F. Pirani, and D. Cappelletti, J. Chem. Phys. **111**, 2620 (1999).
- [11] J. R. Fair and D. J. Nesbitt, J. Chem. Phys. **111**, 6821 (1999).
- [12] J. D. Weinstein, R. deCarvalho, T. Guillet, B. Friedrich, and J. M. Doyle, Nature (London) **395**, 148 (1998); D. Egorov, T. Lahaye, W. Schollkopf, B. Friedrich, and J. M. Doyle, Phys. Rev. A **66**, 043401 (2002).
- [13] J. L. Bohn, Phys. Rev. A **61**, 040702 (2000); A. Volpi and J. L. Bohn, *ibid.* **65**, 052712 (2002).
- [14] A. V. Avdeenkov and J. L. Bohn, Phys. Rev. A **64**, 052703 (2001).
- [15] E. Bodo, E. Scifoni, F. Sebastianelli, F. A. Gianturco, and A. Dalgarno, Phys. Rev. Lett. **89**, 283201 (2002).
- [16] R. C. Forrey, N. Balakrishnan, V. Kharchenko, and A. Dalgarno, Phys. Rev. A **58**, R2645 (1998).
- [17] J. L. Bohn, A. V. Avdeenkov, and M. P. Deskevich, Phys. Rev. Lett. **89**, 203202 (2002).
- [18] J. C. Flasher and R. C. Forrey, Phys. Rev. A **65**, 032710 (2002).
- [19] A. M. Arthurs and A. Dalgarno, Proc. R. Soc. London, Ser. A **256**, 540 (1963).
- [20] R. T. Pack, J. Chem. Phys. **60**, 633 (1974).
- [21] P. McGuire and D. J. Kouri, J. Chem. Phys. **60**, 2488 (1974); P. McGuire, *ibid.* **62**, 525 (1975).
- [22] R. V. Krems, J. Chem. Phys. **116**, 4517 (2002); R. V. Krems, *ibid.* **116**, 4525 (2002).
- [23] H. Rabitz, J. Chem. Phys. **57**, 1718 (1972); G. Zarur and H. Rabitz, *ibid.* **59**, 943 (1973).
- [24] J. M. Hutson and S. Green, MOLSCAT computer code, version 14 (1994), distributed by Collaborative Computational Project No. 6 of the Engineering and Physical Sciences Research Council (UK).
- [25] R. Krems (private communication).
- [26] G. C. Groenenboom and I. M. Struniewicz, J. Chem. Phys. **113**, 9562 (2000).
- [27] R. S. Friedman, J. Quant. Spectrosc. Radiat. Transf. **43**, 225 (1990).
- [28] J. F. Babb and A. Dalgarno, Phys. Rev. A **51**, 3021 (1995).
- [29] P. D. Magill, B. Stewart, N. Smith, and D. E. Pritchard, Phys. Rev. Lett. **60**, 1943 (1988).
- [30] A. J. McCaffery, J. Chem. Phys. **111**, 7697 (1999); S. Clare and A. J. McCaffery, J. Phys. B **33**, 1121 (2000).